Electronic Supplementary Information (ESI)/Supporting information

Simultaneously Improved Stretchability, Stability, and Output Power in Solar Cells via Entanglement Control

*Kangkang Zhou,[a] Dexia Han,[a] Kaihu Xian,[a] Saimeng Li,[a] Mengyuan Gao,[a] Kai Zhang,[a] Bin Zhao,[a] Xin Li,[a] Yu Chen,[b] Yanhou Geng,[a,c] Long Ye *[a]*

[a]School of Materials Science and Engineering, Tianjin Key Laboratory of Molecular Optoelectronic Sciences, Key Laboratory of Organic Integrated Circuits, Ministry of Education, Collaborative Innovation Center of Chemical Science and Engineering (Tianjin), Tianjin University, Tianjin 300350, China

[b]Institute of High Energy Physics, Chinese Academy of Sciences, Beijing 100049, China

[c]Joint School of National University of Singapore and Tianjin University, International Campus of Tianjin University Binhai New City, Fuzhou, Fujian, 350207 China

Experimental Section

Materials: All chemicals were purchased from commercial sources without further purification. PBQx-TCl and PNDI (N2200) were purchased from Solarmer Materials Inc. PYF-IT and PNDIT-F3N were purchased from eFlexPV Limited. PEDOT:PSS (4083) was purchased from the CleviosTM. All solvents were purchased from Sigma Aldrich , Energy Chemical or Heowns.

Molecular weight characterization: Using 1,2,4 trichlorobenzene (TCB) as eluent and polystyrene (PS) as standard, the number average molecular weight (M_n) and weight average molecular weight (M_w) of PNDI were determined by high temperature gel permeation chromatography (GPC) at 150℃.

Device Fabrication: The conventional device structure of Substrate/ PEDOT:PSS/ active layer/ PNDIT-F3N/ Ag was adopted in this study. The rigid device is made on an ITO glass substrate, while the intrinsically stretchable device is on a TPU/AgNWs substrate. Polymer blends were dissolved in chloroform at the total concentration of 14 mg/mL and the optimal D/A ratio was 1:1.2 (w/w). The blend solutions were stirred at 60 °C for 4 h to fully dissolve. Prior to spin-coating the active layer solutions, 2% CN (v/v) was added into the solutions. PNDIT-F3N was dissolved in methanol at the concentration of 0.5 mg/mL with 0.5 v% of acetic acid. Devices were fabricated as follows. First, ITO substrates were treated with UV ozone for 25 min. Then, about 20 nm PEDOT:PSS layers were deposited via spin-coating on the pre-cleaned ITO substrates and annealed at 150 °C for 20 min. Subsequently, the substrates were transferred to the argon-filled glove box. The mixed solutions were spin-coated onto the PEDOT:PSS layers, and the thicknesses of all active layers were about 100 nm. Then the films were treated with thermal annealing at 100 °C for 10 min. PNDIT-F3N was spin-coated on the top of the active layers. Finally, 100 nm thick Ag was deposited on the top of PNDIT-F3N layer under high vacuum. The fabrication process of intrinsically stretchable devices is exactly the same as that of rigid devices except that the top electrode is sprayed with EGaIn (25 wt % In and 75 wt % Ga, then, the EGaIn

mixture was heated at 200 °C for 1 h.). The effective area of the small area cells is about 0.04 cm^2. Thin-films were prepared by spin coating from the toluene solutions.

Electrochemical Properties: The *J-V* measurements were performed via the AAA solar simulator (SS-F5-3A, Enli Technology Co. Ltd, Taiwan) along with AM 1.5G spectra whose intensity was calibrated by the certified standard silicon solar cell at 100 mW/cm^2. The EQE spectra were measured through the Solar Cell Spectral Response Measurement System QE-R3011 (Enli Technology Co. Ltd, Taiwan). The thickness of blend layer was measured via the surface profilometer Bruker Dektak XT.

GIWAXS Characterizations: The samples for GIWAXS measurements were prepared on silicon substrates and the conditions were the same as the device preparation. GIWAXS experiments were carried out at the beamline 1W1A of Beijing Synchrotron Radiation Facility (BSRF) with an incident beam energy at 8 keV and the beamline BL16B1, BL14B1 and BL02U2 of Shanghai Synchrotron Radiation Facility (SSRF) with an incident beam energy at 10 keV. Scattering data were all collected with a fixed grazing angle of 0.2°. The beam center and sample-to-detector distance were calibrated with LaB6.

Morphology Characterizations: The surface morphology of films was measured by a Nanoscope V AFM (Bruker Multimode 8) in tapping mode. The type of AFM cantilever is RTESPA-300, which possesses a k constant of about 40 N/m. The scanning area was 2 μm × 2 μm and the resolution is 256×256 pixels. The TEM images of films were obtained by the JEOL JEM-2100PLUS electron microscope and its accelerating voltage is 200 kV. The magnification of all TEM images is 30K.

Mechanical measurements: FOE tests were carried out using a polarizing microscope (ECLIPSE LV100N POL, Nikon) and a custom-designed tensile stage. The films were coated on glasses (size: 1.7 ×1.7 cm) and then transferred to the PDMS film via water. The crack-onset strains of films were measured by stretching PDMS until the films

started to crack under the observation of a polarized light microscope. Stress-strain curves were acquired using a custom-designed FOW instrument (Auto Tensile Tester, MTM 920, SYSTESTER). In the FOW test, the blend films were coated on precleaned glasses (size: 2 × 2 cm) and then cut into a rectangle shape and transferred to the water surface. The blend films were moved above the PDMS fixture and then glued to the PDMS by lowering the liquid level. The thickness of the neat and blend films is about 100 nm.

The fraction of aggregates relies on the deconvolution of the contribution of non-aggregated chains and aggregates in each spectrum. First, the spectra of CF solutions were normalized to the absorbance at 550 nm. Then, subtracting the spectrum of CN solution (which represents the absorption of non-aggregated chains) from each spectrum, thereby obtaining the absorption of aggregates. Herein, since the absorption of PNDI in CN varies little with molecular weight, the spectrum of P53k sample in CN was subtracted in all cases. Next, integrating the spectra of non aggregated chains and aggregates between 500 and 900 nm, and their areas were termed as Samorph and Saggr, respectively. Finally, since the extinction coefficient of aggregates is 2.5 times that of non-aggregated chains, the fraction of aggregates is given by: [1]

$$aggr\% = \frac{S_{aggr}/2.5}{S_{amorph} + S_{aggr}/2.5} \qquad \text{(Equation S1)}$$

Integrating the spectra between 500 and 900 nm, the areas of non-aggregated chains and aggregates are termed as S_{amorph} and S_{aggr}, respectively.

$$\eta_{sp} = (\eta - \eta_s)/\eta_s \qquad \text{(Equation S2)}$$

where η and η_s are the viscosities of the solution and solvent, respectively.

The 2D PSD of the Fourier transform for the digital TEM images is defined as:[2]

$$PSD(f_x,f_y)=\frac{1}{L^2}\left|\int_0^L\int_0^L e^{-i2\pi xf_x}e^{-i2\pi yf_y}I(x,y)dxdy\right|^2 \quad \text{(Equation S3)}$$

where L is the image size, f_x and f_y are the spatial frequencies along the *x-axis* and *y*-axis, respectively, the relevant range lies between the inverse image size ($1/L$) and the high-frequency limit $N/2L$, and N is the number of pixels per scan line. I(x,y) is the phase contrast intensity of the TEM image. Using this equation, we can obtain a 2D FT image in f_x and f_y. Note, however, that on a large scale the morphology shown on the TEM images are isotropic. As a result, PSD based on polar co-ordinates (r, h) should be a more rigorous tool for scaling analysis. By averaging over h, the PSD can be represented as a function of radial frequencies f to yield the radial 1D PSD graph

$$PSD(f)=\frac{1}{2\pi}\int_0^{2\pi}PSD(f,\theta)d\theta \quad \text{(Equation S4)}$$

In order to quantitatively analyze the phase separation of thin films, we obtain the phase region characteristic size of thin films using the following equation

$$d=\frac{2\pi}{q} \quad \text{(Equation S5)}$$

where q is frequency, d is characteristic size.

$$\frac{1}{T_m}-\frac{1}{T_m^0}=-\frac{RV_{2u}}{\Delta H_{2u}V_{1u}}\left[\frac{lnV_2}{m_2}+\left(\frac{1}{m_2}-\frac{1}{m_1}\right)\times(1-V_2)+\chi_{12}(1-V_2)^2\right] \quad \text{(Equation S6)}^3$$

where T_m and T_m^0 are the melting point of blend and crystalline polymer, respectively. V_{2u}, V_2 and ΔH_{2u} are the molar volume of the repeating units, volume fraction and enthalpy of crystalline polymer respectively. The degree of polymerization, m, is very large, and $V_1 = 1 - V_2$, so equation (1) therefore reduces to

$$\frac{1}{T_m}-\frac{1}{T_m^0}=-\frac{RV_{2u}}{\Delta H_{2u}V_{1u}}\chi_{12}V_1^2 \quad \text{(Equation S7)}$$

where V_1 is volume fraction of the amorphous polymer.

In PNDI blends (M_w>M_c), PNDI with high stretchability and low elastic modulus can act as soft phase, thus Coran-Patel and Davies models can be combined to describe these blends. The equation is as follows:

$$E = \left(1 - V_3^n\right)\left(nV_3 + 1\right)\left(E_u - E_l\right) + E_l \quad \text{(Equation S8)}^{4, 5}$$

$$E_u = E_i\left(1 - V_3\right) + E_3V_3$$

$$E_l = \frac{E_iE_3}{E_3\left(1 - V_3\right) + E_iV_3}$$

Where E_i is the elastic modulus of PBQx-TCl:PYF-IT, and n represents the adjustable parameter, which is related to the degree of softness and hardness. Considering the elastic modulus of PNDI and miscible with PYF-IT, n is determined to be 1. When substituting the relevant values, the curve of Coran Patel-Davies model shows excellent agreement with the experimental data.

$$E = E_m\left(\frac{1 + \zeta_1\eta_1V_1 + \zeta_2\eta_2V_2}{1 - \eta_1V_1 - \eta_2V_2}\right) \quad \text{(Equation S9)}^{6, 7}$$

$$\eta_1 = \frac{E_1/E_m - 1}{E_1E_m + \zeta_1}, \eta_2 = \frac{E_2/E_m - 1}{E_2E_m + \zeta_2}$$

Where ζ_i and m represent the shape factor of fillers and matrix. Since PYF-IT and N2200 (M_w<M_c) are short fibers in the blend membrane, their ζ value is assumed to be 13.3, similar to the previous study. We found that the experimental data were close to the Halpin-Tsai model.

Table S1. PCE and T_{80} lifetime of all-PSCs in previous work and our work.

Blends	PCE_{max} (%)	Annealing temperature (°C)	T_{80} lifetime (*h*)	Reference
PTzBI-Si:N2200	11.2	80	~2000	[8]
PBDTTTPD:N2200	6.67	150	~6	[9]
PBDBT-BV_{20}:N2200-TV_{10}	5.12	80	~7	[10]
PM6:PYF-T-o (1:1.2 blade)	9.2	70	~218	[11]
PM6:PYF-T-o (1:4 spin)	5.2	70	~39	[11]
PM6:PYF-T-o (1:4 blade)	6.4	70	~44	[11]
PM6:PF1-TS4	8.63	85	~20	[12]
PBDB-T:P(BDT2BOY5-Cl)	10.67	100	~80	[13]
PBDB-T:N2200	5.86	100	~500	[13]
PBDT(T)FTAZ:N2200	6.14	150	~200	[14]
PBDT(T)FTAZ-B5:N2200	6.86	150	~240	[14]
PBDT(T)FTAZ-B5:N2200 (UV 5min)	6.43	150	~480	[14]
PBDT(T)FTAZ-B5 N2200 (UV 15min)	5.78	150	~320	[14]
PFBZ:N2200	8.1	150	~180	[15]
PBDB-T:PYF-T	15.68	100	~145	[16]
PBDB-T:PYF-T:PZT	16.37	100	~750	[16]
PM6:PY-IT	15	20~35	~2300	[17]

PM6:PY-IT:PYF-IT	16.6	20~35	~3600	[17]
PM6: PYF-IT	15.1	20~35	~3100	[17]
PM6:PY-V-γ (BC)	16.6	65	~1200	[18]
PM6:PY-V-γ (SD)	17.7	65	~1400	[18]
PBQx-TCl:PYF-IT:P180k	17.1	85	~10600	Our work

Table S2. PCE and strain at $PCE_{80\%}$ of intrinsically stretchable devices in previous work and our work.

Blends	**All-polymer solar cells**	**PCE_{max} (%)**	**Strain at $PCE_{80\%}$**	**Cycles-strain**	**Reference**
PTB7-Th:PCBM		5.32	8.1%	50-20%	[19]
PTB7-Th:N2200	yes	2.02	20.2%	50-20%	[19]
PTB7-Th:ITIC		1.66	10.4%	-	[20]
PTB7-Th:P(NDI2HD-T)	yes	3.00	15.7%	-	[20]
PTzNTz: $PC_{71}BM$		9.70	7.7%	500-37%	[21]
PBDB-T:PCE10:N2200	yes	6.33	11.2%	120-10%	[22]
PM6:Y7		11.2	12.4%	1000-10%	[23]
PM6:PCBM		5.7	5.1%	1000-10%	[23]
PCE12:N2200	yes	5.0	42.3%	1000-10%	[23]
PTB7-Th:IEICO-4F		10.1	12.0%	300-20%	[24]
PM6:Y7:N2200		11.71	19.9%	100-15%	[25]
PhAm5:Y7		12.7	31.6%	120-25%	[26]
PM6:Y6		13.2	~20%	1000-20%	[27]

PM6:BTP-eC9		10.9	~10%	500-20%	[28]
PM6:PY-IT	yes	9.52	~10%	500-20%	[28]
PM6:N2200	yes	3.58	78.4%	500-20%	[28]
PM6:Y6-BO:N2200		10.2	~40%	1000-10%	[29]
PCE12:N2200	yes	6.31	~60%	1000-10%	[29]
PM6-OEG5:BTP-eC9		12.05	22%	150-10%	[30]
PM6:BTP-eC9		10.59	11%	150-10%	[30]
PM6OEG5:Y6-BO:N2200		11.26	~25%	-	[31]
PM6:L8-BO:BTP-eC9		16.23		200-10%	[32]
PBQx-TCl:PYF-IT:P180k	yes	12.3	51.2%	1000-50%	Our work

Table S3. Molecular weight information of PNDI.

	M_n	M_w	PDI
P53k	30.3k	52.5k	1.7
P84k	50.3k	83.8k	1.7
P123k	71.0k	123.4k	1.7
P180k	90.1K	179.5K	2.0
P217k	123.3K	216.8K	1.8
P251k	141.2K	251.2K	1.8

Table S4. The fraction of aggregates of PNDI.

	CN	**P53k**	**P84k**	**P123k**	**P180k**	**P217k**	**P251k**
S	226.7	474.7	489.5	507.6	684.3	725.6	763.9
Aggr%		45.58	46.32	47.22	54.70	56.15	57.41

Table S5. Mechanical property of PNDI.

	Fracture strain (ε_f) (%)	Fracture strength (σ_f) (MPa)	Yield stress (σ_y) (MPa)	Elastic modulus (E_y) (MPa)	Toughness (u_t) (MJ/m^3)
P53k	2.8±0.6	6.9±0.4	5.6±0.4	269.6±5.3	0.10±0.01
P84k	5.7±1.5	9.1±0.8	7.5±0.5	273.3±4.7	0.35±0.02
P123k	7.8±1.7	12.6±1.1	9.8±0.7	306.8±6.9	0.68±0.05
P180k	48.3±3.2	10.5±0.9	10.6±0.9	356.8±7.1	4.57±0.21
P217k	60.5±3.5	11.7±1.2	12.6±1.2	374.1±8.5	6.38±0.32
P251k	64.0±4.2	12.9±1.3	13.0±1.4	408.2±9.4	6.85±0.36

Table S6. Fracture strain of PBQx-TCl:PYF-IT:PNDI with different PNDI content by FOW.

PNDI Content	**0% (%)**	**10% (%)**	**30% (%)**	**50% (%)**	**70% (%)**	**100% (%)**
Ternary-P53k	7.2±0.5	8.2±0.7	9.5±0.8	11.3±1	14.1±1.1	16.2±1.3
Ternary-P84k	7.2±0.3	9.5±0.7	13.9±0.9	17.3±1.1	19.2±1.2	21.4±1.3
Ternary-P123k	7.2±0.3	10.5±0.7	15.3±0.9	19.4±1.2	21.4±1.3	24.4±1.2
Ternary-P180k	7.2±0.3	15.3±0.9	22.3±1.2	27.2±1.4	33.8±1.5	38.8±1.6
Ternary-P217k	7.2±0.3	12.0±1.0	21.4±1.2	28.5±1.3	36.1±1.6	39.5±1.6
Ternary-	7.2±0.3	11.3±0.9	20.3±1.2	29.8±1.4	38.3±1.6	44.1±1.8

P251k						

Table S7. Toughness of PBQx-TCl:PYF-IT:PNDI with different PNDI content by FOW.

PNDI Content	0% (J/g)	10% (J/g)	20% (J/g)	50% (J/g)	70% (J/g)	100% (J/g)
Ternary-P53k	1.92±0.2	2.03±0.4	2.12±0.4	2.62±0.3	2.93±0.5	3.19±0.5
Ternary-P84k	1.92±0.2	2.16±0.3	2.72±0.3	3.62±0.4	3.79±0.5	3.82±0.5
Ternary-P123k	1.92±0.2	2.36±0.3	3.28±0.4	3.94±0.4	4.54±0.5	4.74±0.4
Ternary-P180k	1.92±0.2	4.00±0.4	6.15±0.5	6.26±0.4	6.79±0.5	7.79±0.6
Ternary-P217k	1.92±0.2	2.96±0.3	5.05±0.4	5.64±0.5	5.96±0.6	5.82±0.5
Ternary-P251k	1.92±0.2	3.20±0.3	6.28±0.3	7.19±0.4	7.41±0.4	8.12±0.5

Table S8. Elastic modulus of PBQx-TCl:PYF-IT:PNDI with different PNDI content by FOW.

PNDI Content	0% (MPa)	10% (MPa)	20% (MPa)	50% (MPa)	70% (MPa)	100% (MPa)
Ternary-P53k	1292±35	1082±28	9903±27	608±24	507±21	286±24
Ternary-P84k	1292±35	1127±30	9975±31	684±25	570±27	404±23
Ternary-P123k	1292±35	1142±31	1025±29	717±27	606±26	461±23

Ternary-P180k	1292±35	1196±32	1127±26	784±27	624±25	542±23
Ternary-P217k	1292±35	1235±33	1150±28	866±26	718±24	623±25
Ternary-P251k	1292±35	1242±34	1184±31	899±26	775±28	692±25

Table S9. COS of PBQx-TCl:PYF-IT:PNDI with different PNDI content by FOE.

PNDI Content	**0% (%)**	**10% (%)**	**20% (%)**	**30% (%)**	**50% (%)**	**70% (%)**	**100% (%)**
Ternary-P53k	15.0±0.6	16.1±1.2	16.5±1.4	17.3±1.5	18.2±1.7	20.5±1.9	22.9±2.1
Ternary-P84k	15.0±0.6	17.3±1.3	18.4±1.2	21.9±1.5	26.3±1.6	30.5±1.9	32.9±1.9
Ternary-P123k	15.0±0.6	19.5±1.3	20.1±1.1	22.4±1.2	27.1±1.4	31.9±1.5	34.1±1.6
Ternary-P180k	15.0±0.6	38.0±1.1	53.1±1.4	60.0±1.2	67.3±1.5	75.2±1.6	86.2±1.5
Ternary-P217k	15.0±0.8	32.5±1,2	48.2±1.3	58.0±1.1	73.5±1.3	82.9±1.4	91.3±1.6
Ternary-P251k	15.0±0.6	30.8±1.2	46.6±1.2	57.3±1.5	75.5±1.7	87.1±1.8	95.1±1.9

Table S10. DSC of polymer blends with different PBQx-TCl (P_D) and PYF-IT (P_A) content.

Blend	**Ratio**	**Melting temperature (°C)**	**Enthalpy (J/g)**
P53k:P_D	9:1	310.0	6.2
	8:2	312.0	4.5
P53k:P_A	9:1	288.6	6.1
	8:2	258.5	6.2
P84k:P_D	9:1	317.0	12.7

	8:2	317.7	11.1
P84k:P_A	9:1	307.6	9.4
	8:2	293.0	11.2
P123k:P_D	9:1	318.2	10.5
	8:2	318.9	10.2
P123k:P_A	9:1	310.9	9.5
	8:2	299.3	8.9
P180k:P_D	9:1	316.8	10.3
	8:2	316.9	7.3
P180k:P_A	9:1	308.7	10.5
	8:2	298.9	6.4
P217k:P_D	9:1	314.7	5.7
	8:2	315.3	4.3
P217k:P_A	9:1	309.4	6.7
	8:2	306.1	5.1
P251k:P_D	9:1	307.9	2.1
	8:2	308.7	1.3
P251k:P_A	9:1	303.7	3.1
	8:2	299.5	2.8

Table S11. The rigid and intrinsically stretchable optimal photovoltaic performance of PBQx-TCl:PYF-IT (1:1.2) and PBQx-TCl:PYF-IT:PNDI (1:0.96:0.24).

	Active layer	**V_{OC} (V)**	**J_{SC} (mA/cm^2)**	**FF (%)**	**PCE_{max} (PCE_{avg})[a] (%)**
Rigid all-PSCs	PBQx-TCl:PYF-IT	0.89	22.70	73.6	14.93 (14.75±0.21)
	Ternary-P53k	0.91	22.76	74.0	15.27 (15.04±0.27)
	Ternary-P84k	0.91	22.85	74.3	15.48 (15.31±0.19)
	Ternary-P123k	0.91	23.54	74.7	16.04 (15.89±0.16)
	Ternary-P180k	0.93	24.29	76.5	17.28 (17.02±0.23)
	Ternary-P217k	0.91	22.98	74.6	15.65 (15.57±0.17)
	Ternary-P251k	0.91	22.21	74.0	14.92

					(14.73±0.25)
Intrinsically stretchable all-PSCs	Binary	0.84	18.22	60.3	9.23 (8.87±0.41)
	Ternary-P53k	0.85	18.58	61.2	9.67 (9.25±0.38)
	Ternary-P84k	0.82	18.85	61.0	9.43 (9.04±0.37)
	Ternary-P123k	0.83	19.27	62.2	9.95 (9.46±0.52)
	Ternary-P180k	0.89	20.93	68.7	12.80 (12.35±0.24)
	Ternary-P217k	0.85	19.66	62.3	10.42 (10.21±0.28)
	Ternary-P251k	0.85	19.56	61.3	10.19 (9.92±0.32)

[a]The average PCE values with standard deviations were obtained from 10 individual devices.

Table S12. The corresponding EQE values of PBQx-TCl:PYF-IT (1:1.2) and PBQx-TCl:PYF-IT:PNDI (1:0.96:0.24).

	Binary	**Ternary-P53k**	**Ternary-P84k**	**Ternary-P123k**	**Ternary-P180k**	**Ternary-P217k**	**Ternary-P251k**
J_{cal} **(mA cm^{-2})**	21.65	21.78	22.03	22.69	23.74	22.12	21.36

Table S13. The exciton dissociation probability (P_{diss}) and exciton collection probability (P_{coll}) of PBQx-TCl:PYF-IT (1:1.2) and PBQx-TCl:PYF-IT:PNDI (1:0.96:0.24).

Blends	J_{sat} **(mA cm^{-2})**	J_{sc} **(mA cm^{-2})**	J_{max} **(mA cm^{-2})**	P_{diss}	P_{coll}
PBQx-TCl:PYF-IT	22.94	22.52	20.27	0.9817	0.8838
Ternary-P53k	22.88	22.51	19.29	0.9841	0.8432
Ternary-P84k	22.54	22.06	19.70	0.9786	0.8737
Ternary-P123k	22.63	22.21	19.42	0.9814	0.8581
Ternary-P180k	21.33	21.02	18.61	0.9854	0.8728
Ternary-P217k	22.51	22.12	18.87	0.9826	0.8384
Ternary-P251k	21.82	21.48	19.09	0.9842	0.8747

J_{sat} represents thesaturatio current density.

J_{max} the current density under maximum power output conditions

P_{diss} is defined as the ratio of J_{sc}/ J_{sat}.

P_{coll} is defined as the ratio of J_{max}/ J_{sat}.

Table S14. Intrinsically stretchable optimal photovoltaic performance of PBQx-TCl:PYF-IT:P180k with different P180k content.

P180k Content (%)	**Voc (V)**	**Jsc (mA/cm^2)**	**FF (%)**	**PCE$_{max}$ (PCE$_{avg}$)**	**Strain at PCE$_{80\%}$ (%)**
10%	0.86	19.45	62.1	10.38 (10.05±0.26)	42.1
20%	0.89	20.93	68.7	12.80 (12.35±0.24)	51.3
30%	0.90	19.85	57.8	10.18 (9.91±0.19)	55.5
50%	0.91	14.54	56.3	7.44 (7.19±0.16)	59.6
70%	0.92	10.29	52.1	4.90 (4.75±0.23)	67.5
100%	0.94	8.98	50.6	4.25 (4.07±0.17)	82.3

Table S15. Photovoltaic performance of PBQx-TCl:PYF-IT:P180k (1:0.96:0.24) during stretching.

Strain (%)	**V_{oc} (mV)**	**J_{sc} (mA cm^{-2})**	**FF (%)**	**PCE (%)**	**Effective area (mm^2)**	**P_{out} (mW)**
0	0.89	20.84	66.2	12.28	4.00	0.49
10	0.89	20.34	65.1	12.11	4.22	0.51
20	0.88	19.85	63.4	11.49	4.42	0.51
30	0.87	19.03	61.6	10.66	4.58	0.49
40	0.86	17.77	60.7	9.35	4.70	0.44
50	0.86	16.67	60.0	8.60	4.80	0.41

Table S16. The optimal photovoltaic performance of PM6:PY-IT (1:1.2) and PM6:PY-IT:PNDI (1:0.96:0.24) with different M_w.

	Active layer	**V_{oc} (V)**	**J_{sc} (mA/cm^2)**	**FF (%)**	**PCE$_{avg}$[a] (%)**

Glass substrate	PM6:PY-IT	0.91	23.21	70.2	14.80±0.21
	PM6:PY-IT:P53k	0.92	23.42	70.6	15.13±0.24
	PM6:PY-IT:P84k	0.93	23.52	72.2	15.82±0.17
	PM6:PY-IT:P123k	0.94	23.72	72.4	16.23±0.28
	PM6:PY-IT:P180k	0.95	24.57	74.1	17.21±0.20
	PM6:PY-IT:P217k	0.94	24.04	73.4	16.60±0.15
	PM6:PY-IT:P251k	0.94	23.81	72.5	16.14±0.32
Intrinsically stretchable all-PSCs	PM6:PY-IT	0.85	18.32	58.5	9.21±0.33
	PM6:PY-IT:P53k	0.86	18.45	60.1	9.55±0.31
	PM6:PY-IT:P84k	0.88	18.15	61.2	9.73±0.27
	PM6:PY-IT:P123k	0.89	19.23	60.7	10.41±0.41
	PM6:PY-IT:P180k	0.90	20.32	63.4	11.65±0.36
	PM6:PY-IT:P217k	0.89	20.01	62.1	11.01±0.18
	PM6:PY-IT:P251k	0.88	19.45	61.3	10.38±0.28

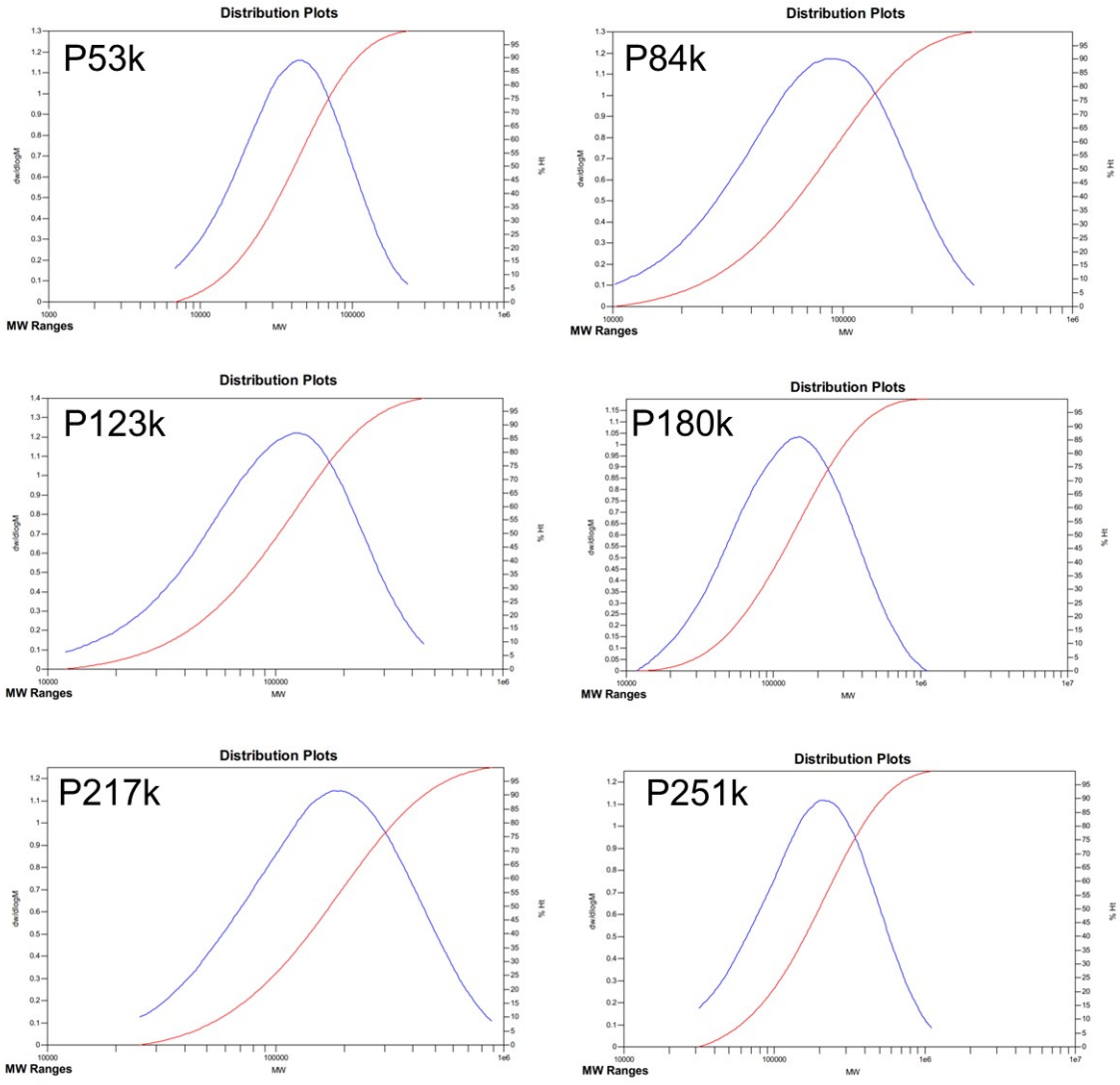

Fig. S1 GPC traces of the PNDI polymers with various M_w.

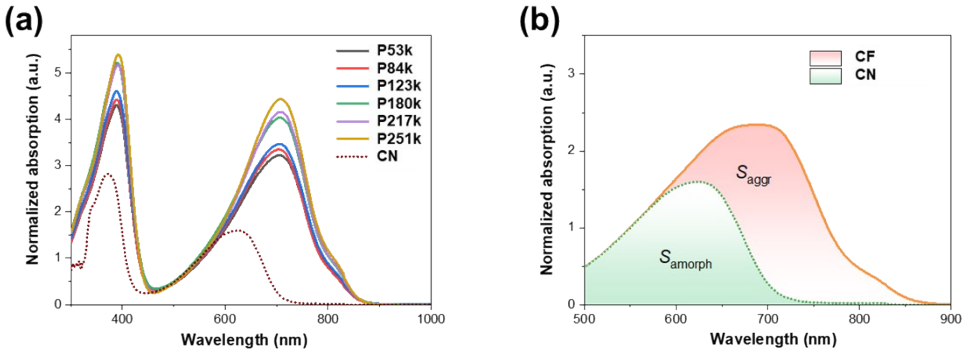

Fig. S2 Deconvolution of the absorption spectra. (a) Normalizing the spectra of P(NDI2OD-T2) in CF solutions to the absorbance at 550 nm. A spectrum of P(NDI2ODT2) in CN solution (non-aggregated state) is also shown for comparison. (b) Subtracting the contribution of non-aggregated chains (CN solution) from a targeted spectrum, the residue is assigned to the contribution of aggregates. Then integrating the spectra between 500 and 900 nm, the areas of non-aggregated chains and aggregates are termed as S_{amorph} and S_{aggr}, respectively.

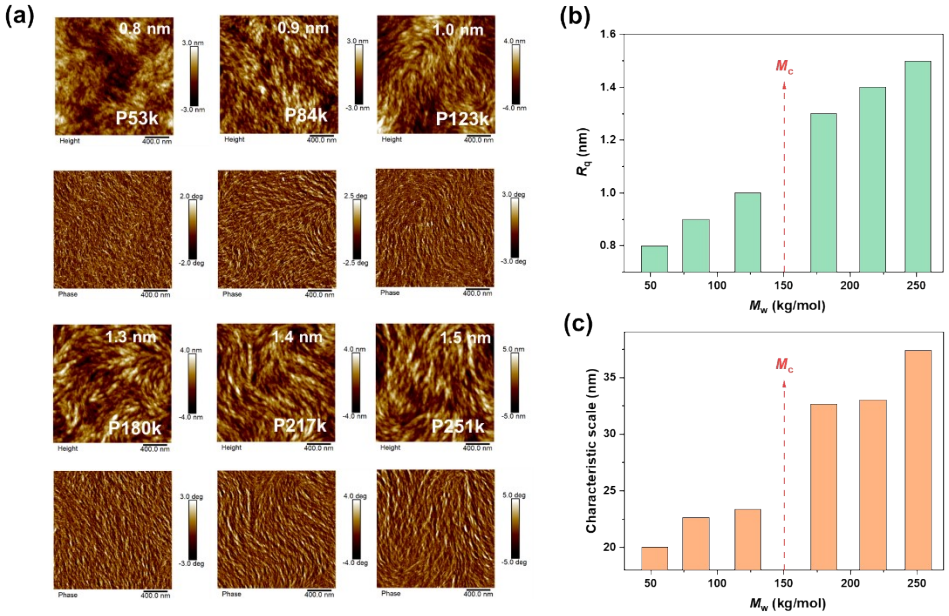

Fig. S3 (a) AFM images, R_q (b) and (c) characteristic scale of PNDI.

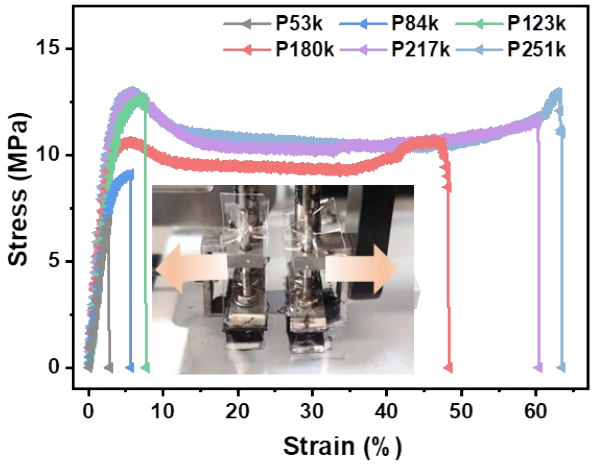

Fig. S4 Stress-strain curves of PNDI.

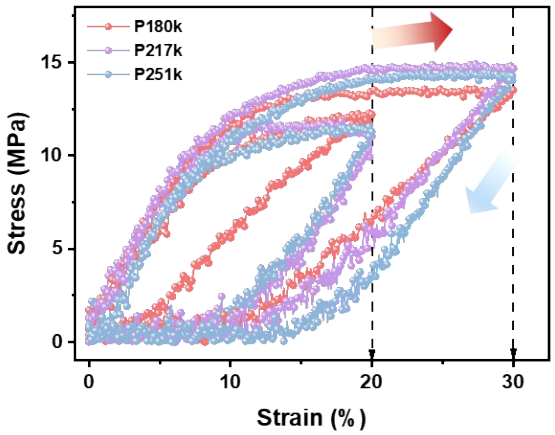

Fig. S5 Tension-recovery curves of PNDI with different molecular weight.

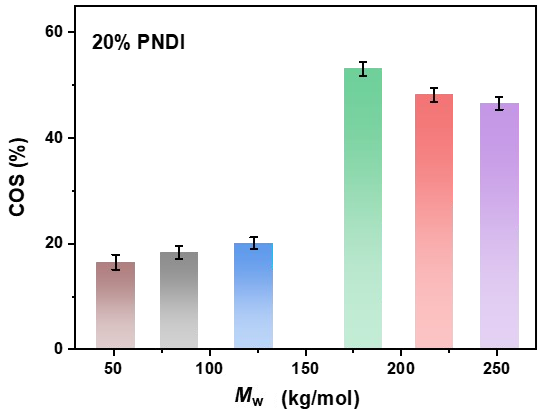

Fig. S6 COS of PBQx-TCl:PYF-IT:PNDI blends with 20% content PNDI.

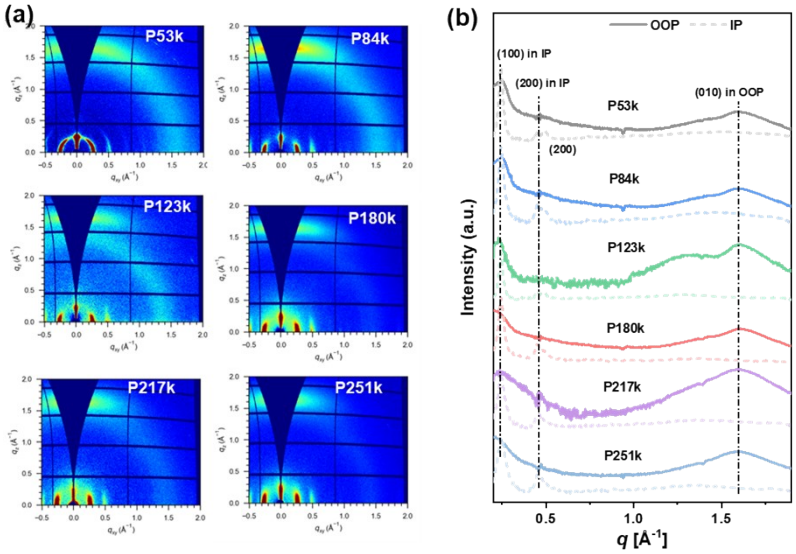

Fig. S7 (a-b) 2D GIWAXS patterns and 1D scattering profiles of PNDI.

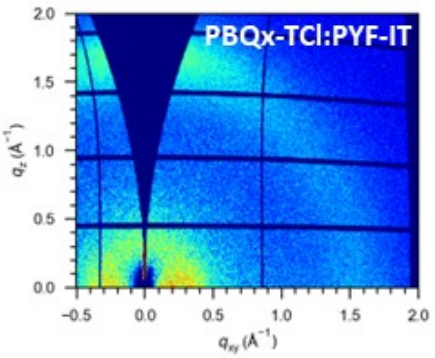

Fig. S8 2D GIWAXS patterns of PBQx-TCl:PYF-IT.

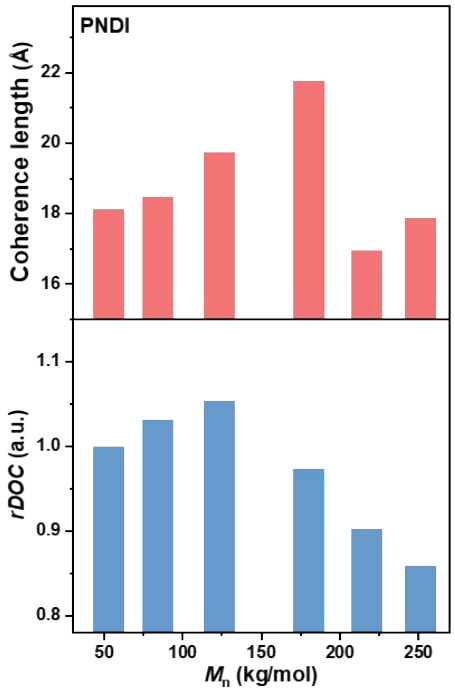

Fig. S9 rDoC and coherence length of PNDI with different molecular weights.

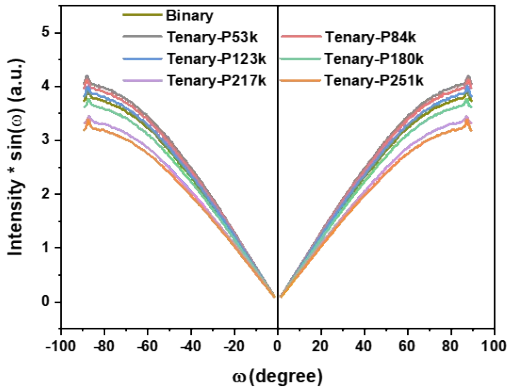

Fig. S10 Pole figures extracted from the (100) diffraction of 2D GIWAXS patterns of ternary blends.

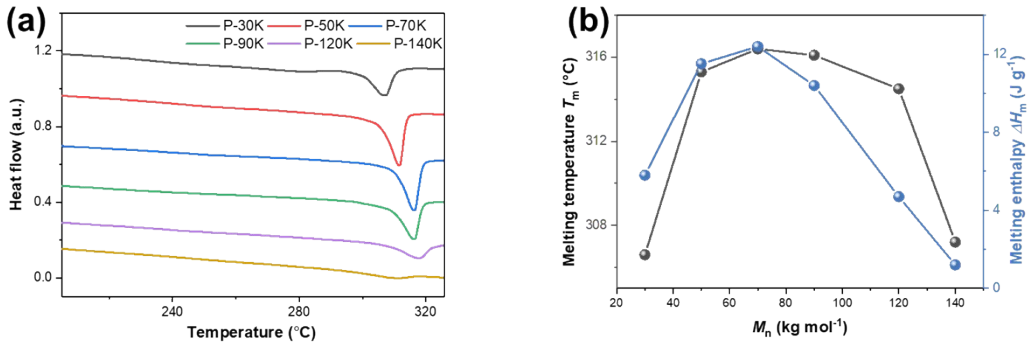

Fig. S11 (a) DSC curves and (b) melting point information of different molecular weight PNDI.

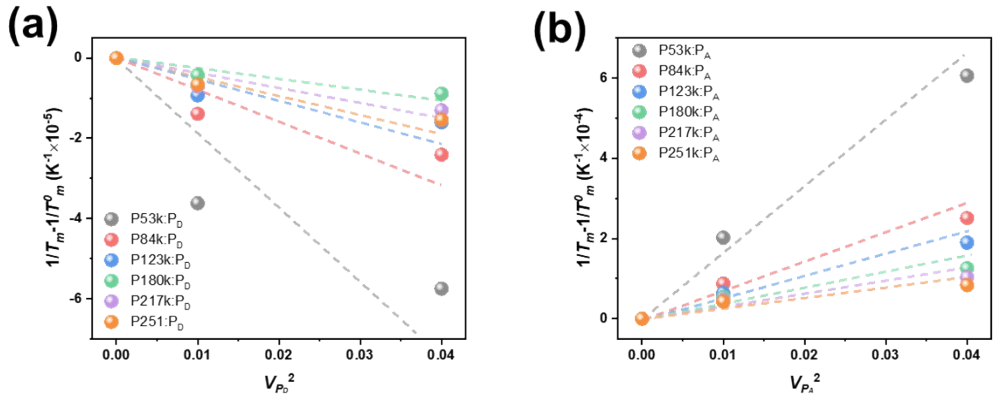

Fig. S12 The $1/T_m$-$1/T^0_m$ depression of PNDI with different M_w as a function of the content of (a) P_D and (b) P_A.

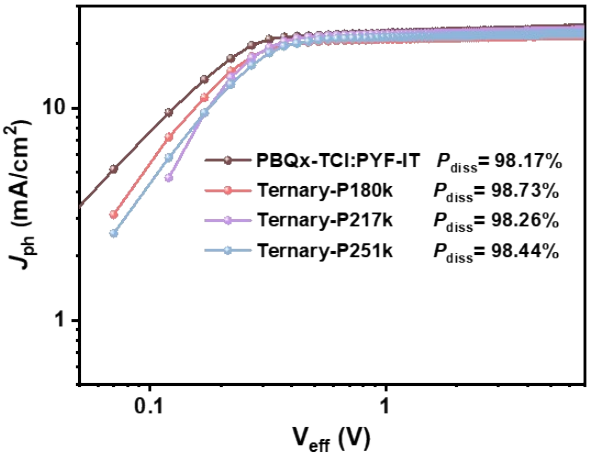

Fig. S13 J_{ph} versus V_{eff} plots of relevant devices.

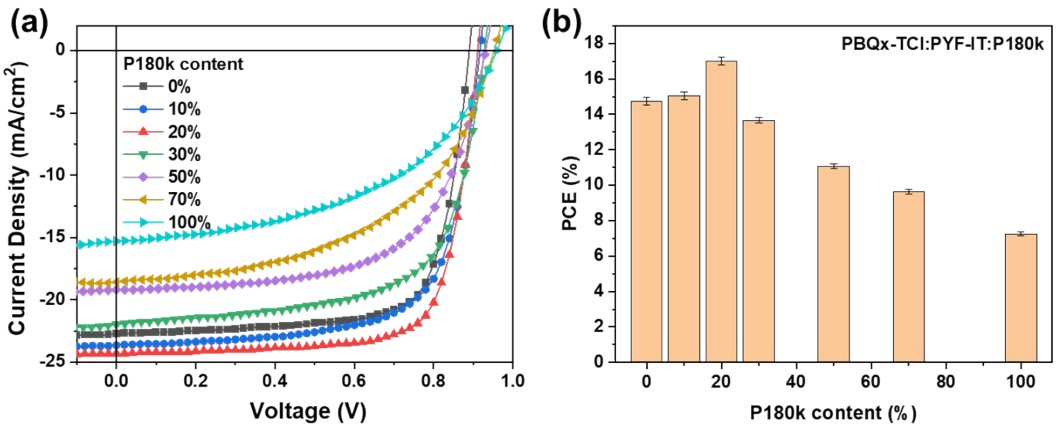

Fig. S14 (a) Optimized J-V curves of PBQx-TCl:PYF-IT:P180k with different P180k content. (b) PCE values of PBQx-TCl:PYF-IT:P180k with different P180k content.

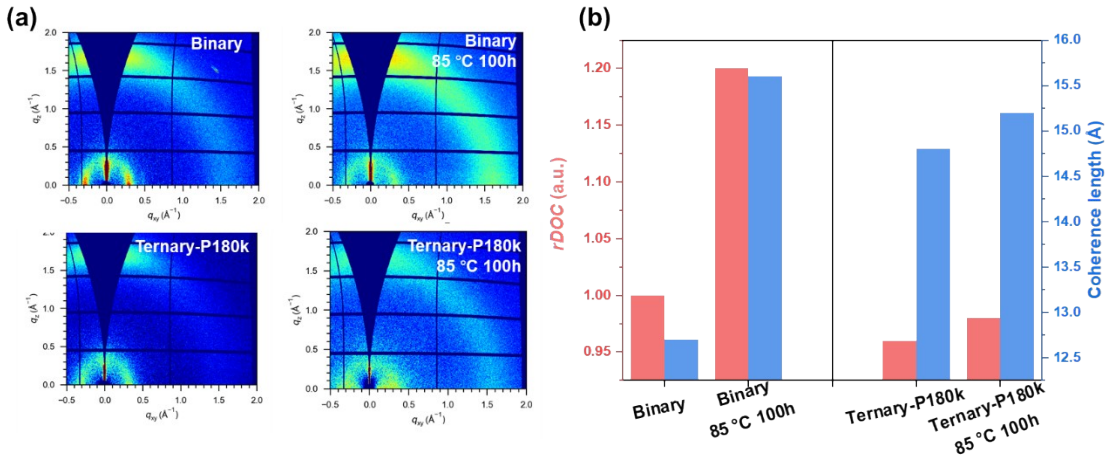

Fig. S15 (a) 2D GIWAXS patterns of binary and ternary-P180k films. (b) coherence length and the rDOC of binary and ternary-P180k films.

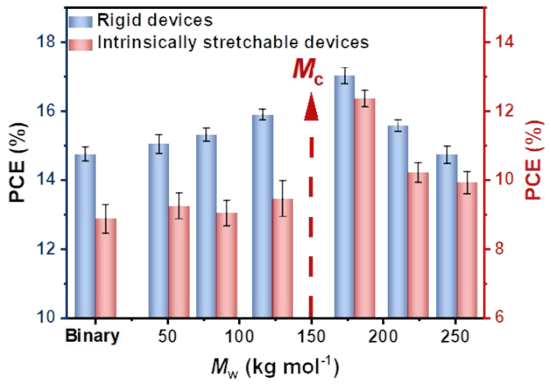

Fig. S16 PCE values of PBQx-TCl:PYF-IT:PNDI.

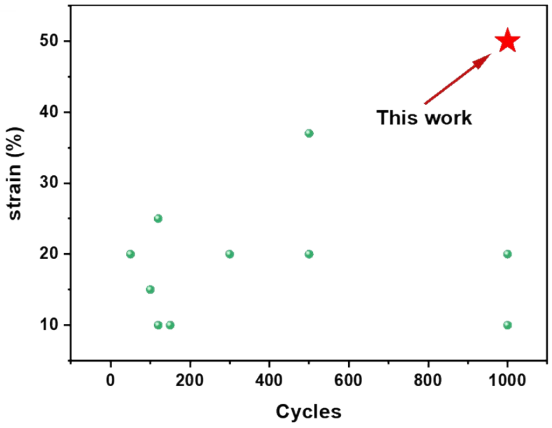

Fig. S17 Tensile strain of IS Ternary-P180kdevices and previous works as a function of cycles.

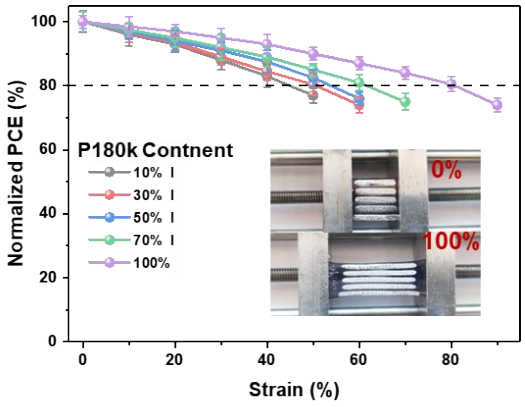

Fig. S18 Plots of normalized PCE versus strain of the Ternary-P180k with different

content.

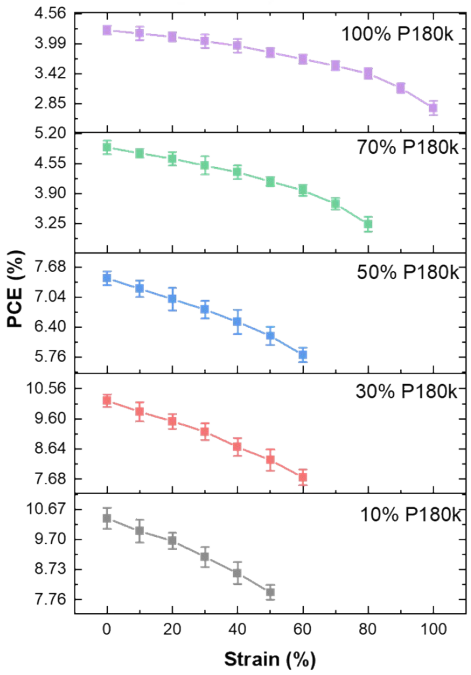

Fig. S19 Actual PCE versus strain of the Ternary-P180k device with different contents of P180k.

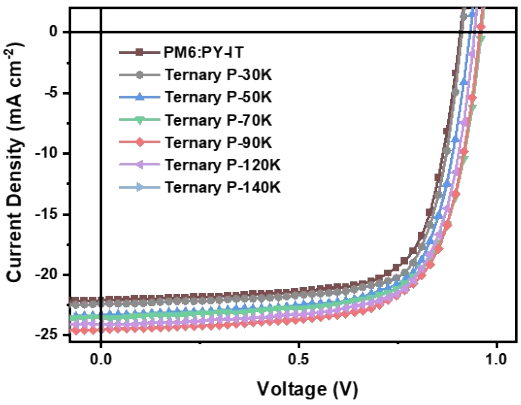

Fig. S20 Optimized *J-V* curves of PM6:PY-IT:PNDI with different M_w.

References

1. K. Zhao, T. Zhang, L. Zhang, J. Li, H. Li, F. Wu, Y. Chen, Q. Zhang and Y. Han,

Macromolecules, 2021, **54**, 10203-10215.
2. W. Ma, C. Yang and A. J. Heeger, *Adv. Mater.*, 2007, **19**, 1387-1390.
3. N. T. and W. T. T., *Macromolecules*, 1975, **8**, 909.
4. C. A. Y. and P. R., *Rubber Chem. Technol.*, 1981, **54**, 91-100.
5. D. W. E. A., *J. Phys. D: Appl. Phys.*, 1971, **4**, 1176.
6. J. C. H. Affdl and J. L. Kardos, *Polym. Eng. Sci.*, 2004, **16**, 344-352.
7. J.-H. Kim, J. Noh, H. Choi, J.-Y. Lee and T.-S. Kim, *Chem. Mater.*, 2017, **29**, 3954-3961.
8. K. Zhang, R. Xia, B. Fan, X. Liu, Z. Wang, S. Dong, H. L. Yip, L. Ying, F. Huang and Y. Cao, *Adv. Mater.*, 2018, **30**, 1803166.
9. T. Kim, J. Choi, H. J. Kim, W. Lee and B. J. Kim, *Macromolecules*, 2017, **50**, 6861-6871.
10. N. Y. Kwon, S. H. Park, H. Kang, Y. U. Kim, H. D. Chau, A. K. Harit, H. Y. Woo, H. J. Yoon, M. J. Cho and D. H. Choi, *ACS Appl. Mater. Interfaces*, 2021, **13**, 16754-16765.
11. X. Rodríguez-Martínez, S. Riera-Galindo, L. E. Aguirre, M. Campoy-Quiles, H. Arwin and O. Inganäs, *Adv. Funct. Mater.*, 2022, **33**, 2213220.
12. Q. Fan, W. Su, S. Chen, T. Liu, W. Zhuang, R. Ma, X. Wen, Z. Yin, Z. Luo, X. Guo, L. Hou, K. Moth-Poulsen, Y. Li, Z. Zhang, C. Yang, D. Yu, H. Yan, M. Zhang and E. Wang, *Angew. Chem. Int. Ed.*, 2020, **59**, 19835-19840.
13. J. W. Lee, C. Sun, B. S. Ma, H. J. Kim, C. Wang, J. M. Ryu, C. Lim, T. S. Kim, Y. H. Kim, S. K. Kwon and B. J. Kim, *Adv. Energy Mater.*, 2020, **11**, 2003367.
14. Z. Lin, L. Zhang, S. Tu, W. Wang and Q. Ling, *Solar Energy*, 2020, **201**, 489-498.
15. W. Su, Y. Meng, X. Guo, Q. Fan, M. Zhang, Y. Jiang, Z. Xu, Y. Dai, B. Xie, F. Liu, M. Zhang, T. P. Russell and Y. Li, *J. Mater. Chem. A*, 2018, **6**, 16403-16411.
16. Z. Li, Y. Liang, L. Chen, J. Chen, F. Peng and L. Ying, *Chem. Eng. J.*, 2023, **452**.
17. K. Xian, K. Zhou, M. Li, J. Liu, Y. Zhang, T. Zhang, Y. Cui, W. Zhao, C. Yang, J. Hou, Y. Geng and L. Ye, *Chinese J. Chem.*, 2022, **41**, 159-166.
18. Y. Wang, H. Yu, X. Wu, D. Zhao, S. Zhang, X. Zou, B. Li, D. Gao, Z. Li, X. Xia, X. Chen, X. Lu, H. Yan, C. C. Chueh, A. K. Y. Jen and Z. Zhu, *Adv. Energy Mater.*, 2022, **12**, 2202729.
19. Y. Y. Yu, C. H. Chen, C. C. Chueh, C. Y. Chiang, J. H. Hsieh, C. P. Chen and W. C. Chen, *ACS Appl. Mater. Interfaces*, 2017, **9**, 27853-27862.
20. Y. T. Hsieh, J. Y. Chen, S. Fukuta, P. C. Lin, T. Higashihara, C. C. Chueh and W. C. Chen, *ACS Appl. Mater. Interfaces*, 2018, **10**, 21712-21720.
21. Z. Jiang, K. Fukuda, W. Huang, S. Park, R. Nur, M. O. G. Nayeem, K. Yu, D. Inoue, M. Saito, H. Kimura, T. Yokota, S. Umezu, D. Hashizume, I. Osaka, K. Takimiya and T. Someya, *Adv. Funct. Mater.*, 2018, **29**, 1808378.
22. Q. Zhu, J. Xue, L. Zhang, J. Wen, B. Lin, H. B. Naveed, Z. Bi, J. Xin, H. Zhao, C. Zhao, K. Zhou, S. Frank Liu and W. Ma, *Small*, 2021, **17**, e2007011.
23. J. Noh, G.-U. Kim, S. Han, S. J. Oh, Y. Jeon, D. Jeong, S. W. Kim, T.-S. Kim, B. J. Kim and J.-Y. Lee, *ACS Energy Lett.*, 2021, **6**, 2512-2518.
24. Z. Wang, M. Xu, Z. Li, Y. Gao, L. Yang, D. Zhang and M. Shao, *Adv. Funct. Mater.*, 2021, **31**, 2103534.
25. J. W. Lee, G. U. Kim, D. J. Kim, Y. Jeon, S. Li, T. S. Kim, J. Y. Lee and B. J. Kim, *Adv. Energy Mater.*, 2022, **12**, 2200887.
26. J. W. Lee, S. Seo, S. W. Lee, G. U. Kim, S. Han, T. N. Phan, S. Lee, S. Li, T. S. Kim, J. Y. Lee and B. J. Kim, *Adv. Mater.*, 2022, **34**, 2207544.

27. Z. Wang, D. Zhang, M. Xu, J. Liu, J. He, L. Yang, Z. Li, Y. Gao and M. Shao, *Small*, 2022, **18**, 2201589.
28. J. Huang, Z. Lu, J. He, H. Hu, Q. Liang, K. Liu, Z. Ren, Y. Zhang, H. Yu, Z. Zheng and G. Li, *Energy Environ. Sci.*, 2023, **16**, 1251-1263.
29. S. Lee, Y. Jeon, S. Y. Lee, B. S. Ma, M. Song, D. Jeong, J. Jo, G. U. Kim, J. Lee, T. S. Kim, B. J. Kim and J. Y. Lee, *Adv. Energy Mater.*, 2023, **13**, 2300533.
30. J. W. Lee, C. Lim, S. W. Lee, Y. Jeon, S. Lee, T. S. Kim, J. Y. Lee and B. J. Kim, *Adv. Energy Mater.*, 2022, **12**, 2202224.
31. H. J. Kwon, G. U. Kim, C. Lim, J. K. Kim, S. S. Lee, J. Cho, H. J. Koo, B. J. Kim, K. Char and J. G. Son, *ACS Appl. Mater. Interfaces*, 2023, **15**, 13656-13667.
32. X. Zheng, X. Wu, Q. Wu, Y. Han, G. Ding, Y. Wang, Y. Kong, T. Chen, M. Wang, Y. Zhang, J. Xue, W. Fu, Q. Luo, C. Ma, W. Ma, L. Zuo, M. Shi and H. Chen, *Adv. Mater.*, 2023, **36**, 2307280.